processes

MDPI

Article

Experimental Study on Permeability Variations in Fractured Coal Under Stress Changes in the Mining Area of the Ordos Basin, North China

Jingjing Huo [1], Lihong Jin [2,*], Rui Li [3,*], Baoke Yang [3] and Le Zhang [3]

[1] Sijiazhuang Coal Mine, Lu'An Chemical Group Co., Ltd., Yangquan 045000, China; hjj_sjz@163.com
[2] College of Modern Science and Technology, China Jiliang University, Yiwu 322002, China
[3] State Key Laboratory of Coal Mine Disaster Dynamics and Control, Chongqing University, Chongqing 400044, China; y17673204912@163.com (B.Y.); zl569422673@163.com (L.Z.)
* Correspondence: 202120021026@cqu.edu.cn (L.J.); lirui@cqu.edu.cn (R.L.)

Abstract

Deep coalbed methane (CBM) reservoirs are characterized by high in situ stress, and the effective stress during CBM production is significant, leading to substantial damage to reservoir permeability. Studying the variation patterns of coal permeability during stress unloading is crucial for revealing the mechanisms by which CBM stimulation through slotting and cavity creation modifies in situ stress. To understand the permeability variations in fractured coal under stress changes, gas seepage experiments were conducted using seven deep coal samples obtained from the Linxing–Shenfu mining area in the Ordos Basin of North China. Through these experiments, permeability variations in coal under different confining, axial, and gas pressures were investigated, and their implications for permeability enhancement through hydraulic slotting in deep coal seams were analyzed. The results show that during loading, permeability decreases with increasing effective stress, and the rate of permeability damage increases. During unloading, the changes in coal permeability transition from slow to rapid, with the stress sensitivity coefficient increasing and the stress sensitivity becoming more pronounced. Regardless of the loading or unloading process, lower axial pressure leads to higher permeability, greater permeability recovery and damage rate, a larger stress sensitivity coefficient, and stronger stress sensitivity of the coal. For every 4 MPa decrease in the axial pressure, the permeability increases by approximately 0–10%, and the permeability recovery rate increases by about 6%. This is because the lower axial pressure reduces the effective stress acting on the coal matrix and fractures, thereby widening the flow channels and enhancing both the permeability and its recovery capacity. In addition, for every 0.3 MPa increase in the gas pressure, the permeability increases by approximately 10–50%, and the permeability recovery rate increases by about 20%. This indicates that elevating pore pressure effectively counteracts effective stress, expands fracture apertures, and promotes fracture connectivity. This work demonstrates that fractured coal is highly sensitive to stress and that stress relief plays a crucial role in enhancing the permeability of deep coal seams.

Keywords: deep coalbed methane; in situ stress; effective stress; permeability

Check for updates

Academic Editor: Ye Huang

Received: 26 February 2026
Revised: 2 April 2026
Accepted: 4 April 2026
Published: 8 April 2026

Copyright: © 2026 by the authors. Licensee MDPI, Basel, Switzerland. This article is an open access article distributed under the terms and conditions of the Creative Commons Attribution (CC BY) license.

1. Introduction

The exploration and development of coalbed methane (CBM) can significantly enhance energy security, reduce greenhouse gas emissions, and promote clean energy transition [1].

Deep CBM reservoirs, typically located at depths exceeding 1500 m, represent a critical yet challenging frontier for unconventional energy development. These reservoirs are characterized by unique geomechanical conditions, including high in situ stress gradients, elevated pore pressures, and complex geological structures [2]. The permeability of deep coal seams, which fundamentally controls gas flow dynamics and economic viability, exhibits extreme sensitivity to effective stress variations [3]. This stress dependency stems from the dual-porosity nature of coal, in which natural fracture networks serve as the primary conduits for fluid flow [4]. During gas extraction, reservoir pressure depletion increases the effective stress acting on the coal matrix, leading to progressive cleat compression and a significant reduction in permeability—often by several orders of magnitude. This phenomenon poses substantial challenges to sustainable gas production from deep CBM reservoirs, particularly impacting the long-term effectiveness of stimulation techniques such as hydraulic fracturing and hydraulic slotting [5,6]. Understanding the intricate relationship between stress evolution and permeability dynamics in fractured coal systems is therefore paramount for optimizing recovery strategies and ensuring project economics in these demanding subsurface environments [7–10].

The critical influence of stress on coal permeability has been the subject of extensive research over the past few decades. A significant conceptual advance was the development of permeability models that explicitly incorporate effective stress. The classic work by Gray (1987) and subsequent models by Palmer and Mansoori (1998) and Shi and Durucan (2004) provided analytical solutions for permeability evolution in coal under uniaxial strain conditions, which are often assumed for reservoir-scale behavior [11–13]. These models elegantly relate permeability to matrix shrinkage and cleat compression, highlighting the competing mechanisms that control permeability during production. Experimental investigations have paralleled these theoretical developments. Harpalani and Chen (1997), Robertson and Christiansen (2007), and Chen et al. (2013) systematically measured the permeability of intact coal cores under various confining pressures and pore pressures, consistently demonstrating an exponential or power-law decline in permeability with increasing effective stress [14–16]. More recent work has expanded into the different stress conditions and behavior of fractured coal. Researchers such as Wang et al. (2014) and Porfido et al. (2021) used triaxial systems to study how permeability varies with different stresses (the difference between axial and confining stress), revealing more complex, non-monotonic behaviors, including potential permeability recovery or an increase during shear dilation along natural or induced fractures [17,18]. The advent of advanced imaging techniques, such as micro-computed tomography (μ-CT), has enabled visualization of fracture deformation in situ, providing unprecedented insights into the micromechanical processes governing flow [19,20].

Recent investigations have significantly advanced our understanding of stress–permeability coupling in coal reservoirs. Contemporary research has demonstrated through advanced triaxial experiments that permeability evolution in fractured coal follows distinct hysteresis patterns during cyclic loading–unloading stress paths, highlighting irreversible damage accumulation [21,22]. A novel multiphysics model was developed to successfully predict permeability anisotropy in deep coal seams under true triaxial stress conditions [23]. Zhou et al. (2020) investigated the coupled effects of gas adsorption/desorption and stress cycling on fracture connectivity using 3D printed coal analogs with controlled fracture geometries, providing new insights into matrix–fracture interactions [24]. The integration of digital rock physics and machine learning has enabled more accurate permeability predictions from limited core data by identifying key morphological descriptors of fracture networks that control stress sensitivity [25]. Despite these significant advancements, criti-

cal knowledge gaps remain regarding the permeability behavior of fractured coal under realistic, anisotropic stress conditions representative of deep reservoirs [26].

China has abundant deep CBM resources, with onshore CBM resources buried deeper than 1500 m accounting for approximately 71% of the country's total onshore CBM resources, and those buried deeper than 2000 m accounting for about 57%. The CBM resources at depths exceeding 2000 m in the Ordos Basin amount to 12.99 $\times$ 10^{12} m^3, indicating tremendous development potential [27]. In 2021, the CBM output from the eastern margin of the Ordos Basin accounted for 21% of the national CBM production that year [28]. Due to the characteristics of deep coal seams in the study area, such as poor pore connectivity, low matrix permeability, and high effective stress, the development faces numerous challenges that severely constrain the efficient exploitation of deep CBM [29,30]. A previous study revealed that increasing in situ stress exponentially exacerbates CH_4 desorption hysteresis in coal by compressing fractures, reducing pressure gradients, and weakening the driving force required to overcome adsorption potential, thereby limiting recoverable gas [31]. Hydraulic slotting uses high-pressure water jets to cut and break coal rock, forming hydraulic slots that increase the free surface of the borehole. This enables rapid and extensive pressure relief in the coal mass, thereby enhancing the internal permeability of the coal seam and reducing its internal pressure [32]. The high-pressure water jet disrupts the integrity of the coal mass during cutting, weakening its ability to support the overlying strata and effectively alleviating stress concentrations within the slotted area. The free surface of the slot relieves confining pressure, causing concentrated stress to shift toward the outer areas of the slots and the coal between slots [33]. As a result, coal permeability significantly increases, promoting gas desorption and flow. However, there is a lack of systematic experimental data to describe the influence of effective stress on permeability evolution in deep CBM reservoirs on the eastern margin of the Ordos Basin. These limitations hinder the development of predictive models capable of accurately simulating post-stimulation production decline in deep, stressed coal seams.

To understand the changes in coal permeability under stress relief and to quantify the relationship between alterations in stress states in different directions and the permeability of fractured coal, gas seepage experiments are conducted using seven coal samples (six fractured coal samples and one intact coal sample) obtained from the Linxing–Shenfu mining area in the Ordos Basin of North China under varying stress states. The core methodology employs a triaxial stress-seepage coupling apparatus to conduct rigorous flow experiments. An artificially created fracture with controlled orientation is introduced into each specimen. Permeability variations in coal under different confining, axial, and gas pressures are investigated, and their implications for permeability enhancement through hydraulic slotting in deep coal seams are analyzed. Furthermore, the permanence of permeability damage and the recovery rates are investigated through loading and unloading cycles. The aim of this mechanistic study is to provide foundational data for improving the stimulation designs and production strategies for deep, stress-sensitive CBM reservoirs.

2. Experimental Equipment and Methods

2.1. Experimental Samples

During the experiment, coal samples were split to simulate fractured coal rock, allowing the study of how the permeability of fractured coal samples varies with effective stress. The coal samples used in this experiment were all sourced from the Linxing–Shenfu mining area. The main coal seams in the study area are the Nos. 8 + 9 coal seams, with burial depths ranging from 1087 to 2102 m and an average depth of 1800 m. The reservoir pressure of the coal seams mostly ranges from 10.5 to 20.6 MPa, with an average of 18.6 MPa. Porosity varies from 4.23% to 6.79%, averaging at 5.92% [34]. The permeability of the coal

rock is generally less than 0.1 mD, indicating a typical low-porosity, ultra-low-permeability reservoir. The gas content of the deep coal seams in the study area ranges from 8.00 to 30.94 m^3/t, with an average of 15 m^3/t, and the gas saturation ranges from 80% to 120% [35]. Due to geological factors, significant differences in horizontal distribution occur. The vitrinite reflectance of the coal seams increases from 1.01% in the east to 2.10% in the west, indicating medium-rank coal characteristics. In some areas, influenced by the thermal effects of magmatic activity from the Middle Jurassic to the Early Cretaceous Zijinshan rock mass, the vitrinite reflectance exceeds 3.0%, forming a distribution area of high-rank coal.

The selected coal samples were extracted along the parallel bedding planes of the coal rock using a laboratory coring machine, followed by cutting and grinding of the obtained cores. According to the requirements of the experimental apparatus, the coal rock was processed into standard cylindrical specimens with a diameter of 50 mm and a height of 100 mm, as shown in Figure 1. The selected coal samples were placed in a drying oven at 105 °C for 24 h. The mass of the samples was periodically measured until no further weight change occurred. The samples were then sealed with plastic wrap to prevent the initial moisture content from influencing the experiment. Seven samples were used to conduct this experiment, including six fractured coal samples and one intact coal sample. The intact coal samples showed no obvious fractures on the surface (Figure 1a). The tensile strength of coal is very low, making it highly prone to fracturing and crack formation. Using the Brazilian splitting test apparatus, a linear load was applied along the diametrical direction of the cylindrical coal sample. Due to the presence of numerous bedding planes distributed along the diametrical direction, the applied load readily induced splitting of the specimen along the diametrical direction, resulting in the formation of fractures. As the sample splits along the coal bedding planes, the fracture surfaces were relatively smooth and could be readily rejointed. The split coal samples exhibited distinct fractures that vertically penetrated the samples (Figure 1b).

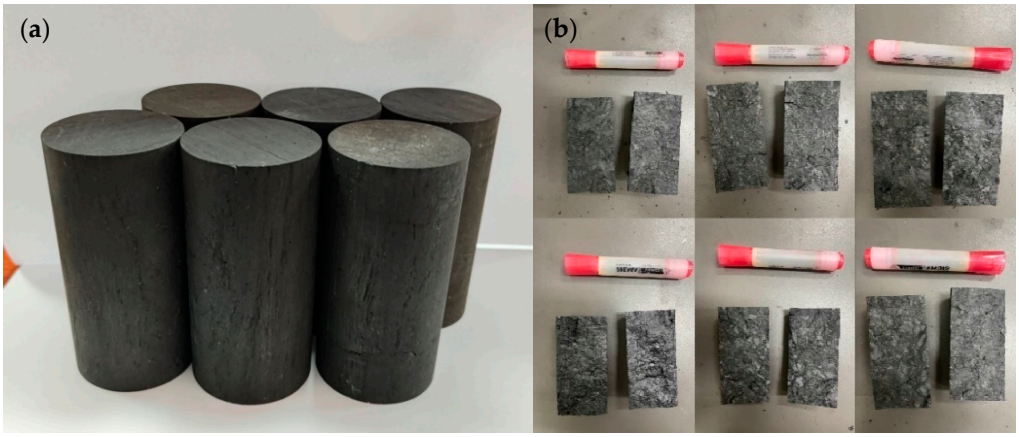

Figure 1. Samples without and with pre-existing fractures: (**a**) samples without fractures; (**b**) samples with pre-existing fractures.

By conducting proximate and XRD analyses, the fundamental properties and coal quality of the coal rock were assessed to lay the foundation for further research. The coal samples used in this experiment were all collected from a coal mine in the Linxing–Shenfu mining area. Structurally intact large pieces of coal rock were collected on-site underground, and cores were extracted from coal blocks with good integrity. The XRD test was conducted using the PANalytical X'Pert Powder high-efficiency conventional powder X-ray diffractometer at the Analytical and Testing Center of Chongqing University, Chongqing, China. The test results are shown in Table 1. An analysis of the XRD results revealed that the coal samples had a high carbonate mineral content and a low silicate mineral content.

Proximate analysis was performed using a box-type resistance furnace. Based on the test results, the coal samples were classified as bituminous coal, characterized by a low ash content and a high volatile matter content (Table 2).

Table 1. XRD analysis.

Quartz/%	Kaolinite/%	Calcite/%	Dolomite/%	Others/%
22.40	18.00	42.40	17.20	0

Table 2. Industrial analysis.

Moisture/%	Ash/%	Volatiles/%	Fixed Carbo/%
13.53	9.32	33.80	43.34

2.2. Experimental Equipment

The experiment utilized the RLW–2000 coal and rock permeability measurement device from the State Key Laboratory of Coal Mine Disaster Dynamics and Control at Chongqing University, Chongqing, China, as shown in Figure 2. The testing apparatus primarily consists of a control system, an axial loading system, a confining pressure system, a drag system, a temperature control system, and a computer system. The maximum axial loading capacity is 2000 kN, with a maximum confining pressure of 80 MPa, a maximum gas pressure of 6 MPa, and a maximum temperature of 120 °C. This equipment can measure the permeability of coal and rock under different gas pressures, loading temperatures, and stress paths.

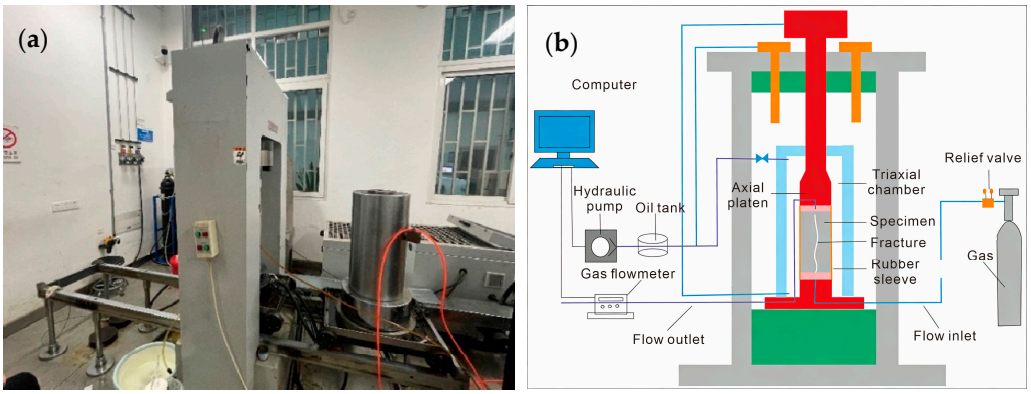

Figure 2. Schematic diagram of the RLW-2000 coal and rock permeability measurement device: (**a**) physical image of the testing apparatus; (**b**) schematic diagram of equipment connections.

The experiment was conducted under indoor conditions at a temperature of 20 °C and atmospheric pressure (0.1013 MPa). Assuming that gas flow in the coal sample is an isothermal process and obeys Darcy's law, the formula used to calculate permeability K is shown in Equation (1):

$$K = \frac{2Q\mu p_2 L}{A(p_1^2 - p_2^2)} \quad (1)$$

In Equation (1), K is the instantaneous permeability of the coal rock in mD; Q is the instantaneous flow rate of coal rock permeation in cm^3/s; μ is the dynamic viscosity of gas under the measurement conditions, taken as 0.017×10^{-3} Pa · s; L is the length of the specimen in cm; A is the cross-sectional area of the coal sample in cm^2; p_1 is the gas pressure at the inlet end, MPa; and p_2 is the gas pressure at the outlet end, taken as atmospheric pressure due to the connection to the atmosphere.

Effective stress is the difference between the confining pressure acting on the coal seam and the fluid pressure within its pores or fractures. In this experiment, the determination of effective stress was altered by adjusting the confining pressure. Therefore, the change in the effective stress is equivalent to the change in the confining pressure.

2.3. Experimental Procedures

(1) Sample Installation. Place metal gaskets on the top and bottom ends of the dried specimen. Secure the specimen inside the instrument chamber, cover it completely with a heat-shrink tube, and heat it using a heat gun. Fasten the specimen with metal retaining rings at positions approximately 1 cm from both end faces. Install the prepared specimen onto the bottom platen of the triaxial chamber and connect the axial extensometer and radial sensors. Attach the oil and gas inlet pipelines to the instrument. Check the airtightness of the equipment and evacuate gases from the specimen using a vacuum pump.

(2) Loading Process. Using the computer control program, apply axial pressure to the set value at a rate of 0.01 MPa/s and in increments of 0.5 MPa. Then, fill the chamber with oil and apply confining pressure to the set value at the same rate and increments. Next, open the gas inlet valve, close the gas outlet valve, and set the inlet pressure to allow the working gas to fully adsorb into the coal sample. After the adsorption equilibrium is reached, open the gas outlet valve. Maintain a stable flow rate and measure it with a gas flow meter. The adsorption capacity of coal for CH_4 is significantly higher than that for N_2. Therefore, N_2 was selected as the experimental gas in this study to minimize the influence of coal rock adsorption deformation on its permeability to the greatest extent.

(3) Unloading Process. Unload the confining pressure of the coal sample using the computer control program. Set the unloading rate of the confining pressure to 0.01 MPa/s, and unload it in increments of 0.5 MPa until the predetermined target value is reached. During this process, measure the flow rate using a gas flow meter.

(4) Experiment Termination. After stopping the gas supply, disconnect the gas inlet pipeline from the equipment. First, unload the confining pressure to 0 MPa, and then unload the axial pressure to 0 MPa. Open the oil return system and allow it to operate for 1 h before disconnecting the oil inlet pipeline from the equipment. Remove the specimen from the triaxial chamber, detach the sensors from the specimen, and clean the equipment. Export the data from the computer for subsequent analysis. Based on the stress conditions in the study area and the parameter conditions of the experimental equipment, the initial confining, axial, and gas pressure parameters for different samples were set, as shown in Table 3.

Table 3. Experimental scheme.

Sample Number	Initial Confining Pressure (MPa)	Axial Pressure (MPa)	Gas Pressure (MPa)
1	10	10	1
2	10	14	1
3	10	18	1
4	10	14	1
5	10	14	0.7
6	10	14	0.4

3. Results and Discussion

3.1. Influence of Axial and Gas Pressures on Permeability Variation

Unloading was performed on intact and fractured coal samples within the same range, and permeability variation curves were plotted, as shown in Figure 3a. When the confining pressure was 10 MPa, the permeability of the intact coal samples was approximately 0.007 mD, while that of the fractured coal samples was approximately 0.078 mD, which is 11.143 times that of the intact coal samples. When the confining pressure was 3 MPa, the permeability of the intact coal samples was approximately 0.017 mD, while that of the fractured coal samples was approximately 0.146 mD, which is 8.588 times that of the intact coal samples. These results indicate that, under the same stress conditions, slotting in coal rock can increase permeability by several times, demonstrating the significant effectiveness of slotting in enhancing coal rock permeability. Additionally, when the confining pressure was unloaded from 10 MPa to 3 MPa, the permeability of the intact coal samples increased by 2.429 times, while that of the fractured coal samples increased by 1.872 times. This suggests that altering the confining pressure in coal seams can significantly enhance coal seam permeability.

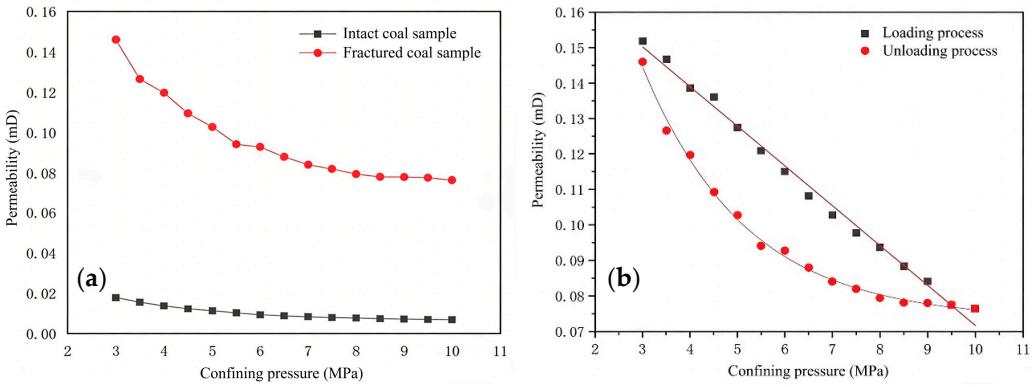

Figure 3. Permeability changes in coal samples: (**a**) permeability changes in the initial and fractured coal samples; (**b**) fitting diagram of permeability with confining pressure.

Figure 3b shows the variation in permeability with confining pressure for fractured coal samples during confining pressure loading and unloading. At a confining pressure of 3 MPa, the permeability of the coal rock is 0.152 mD. When the confining pressure increases to 10 MPa, the permeability of the coal rock drops to 0.076 mD, representing a 50% decrease. An increase in the confining pressure raises the effective stress, constraining the deformation of the coal. Under stress, pores and fractures close to a certain extent, narrowing the coal seepage channels. This increases the resistance to gas flow through the coal sample, leading to a decrease in its permeability as the confining pressure increases.

As the confining pressure decreases, the permeability of the coal rock continuously increases. When the confining pressure is reduced from 10 MPa to 6 MPa, the coal rock's permeability increases to 0.093 mD, representing a 22.37% increase. When the confining pressure is reduced to 3 MPa, the coal rock's permeability is 0.146 mD, representing an increase of 92.11%. The rate of permeability change accelerates over time. This is because the internal pores and fractures in the coal rock gradually open, enhancing CBM flow through the coal sample. In other words, there is a clear negative correlation between coal rock permeability and confining pressure. The aforementioned phenomena indicate that the internal pore and fracture structures of coal rock are highly sensitive to stress. Changes in stress significantly affect these structures, leading to substantial variations in the permeability of the coal sample itself.

Figure 4 shows the stress–strain curve of a fractured coal sample under 1 MPa gas pressure and 10 MPa axial pressure during confining pressure loading and unloading. When the axial pressure is constant, as the confining pressure increases, the radial deformation of the coal sample first increases rapidly and then increases slowly, while the axial deformation remains unchanged. The coal rock compresses, fractures close, and the permeability of the coal sample decreases. Conversely, as the confining pressure decreases, the radial deformation of the coal sample first decreases slowly and then decreases rapidly, while the axial deformation remains unchanged. The coal expands, fractures open, and the coal sample's permeability increases. Under the same confining pressure, the deformation of the coal sample during loading is greater than that during unloading. This is due to the irreversible deformation generated in the coal sample.

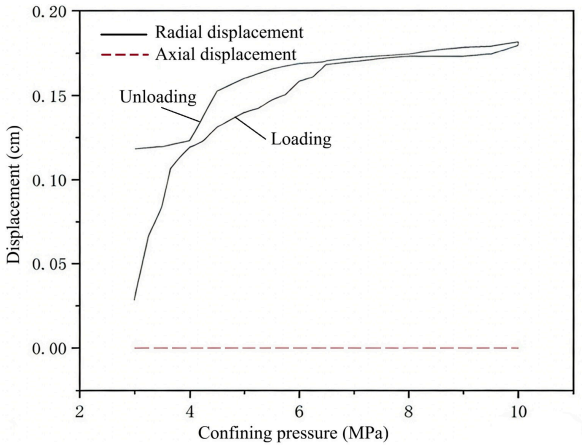

Figure 4. Displacement curves.

Therefore, it can be observed that as the confining pressure increases, the natural fractures in the coal sample gradually close, and the permeability of the coal body gradually decreases. This further demonstrates that during CBM extraction, depressurizing the coal seam can effectively enhance coal permeability.

To further analyze the relationship between permeability and confining pressure, curve fitting was performed, as shown in Figure 3b. The specific fitting results are as follows:

The experimental results obtained during the loading process were fitted using a linear model (Equation (2)):

$$y = -0.0116x + 0.186 \quad (2)$$

Equation (2) indicates that during the loading process, the relationship between the permeability change and confining pressure can be fitted with a linear function. Therefore, under a constant injected gas pressure, the confining pressure during loading exhibits a linear relationship with permeability.

The experimental results obtained during the unloading process were fitted using an exponential function:

$$y = 0.2493e^{-\frac{x}{2.156}} + 0.073 \quad (3)$$

Equation (3) indicates that, during the unloading process, the relationship between the permeability change and confining pressure can be fitted with an exponential function. Therefore, under a constant injected gas pressure, the confining pressure during unloading exhibits a negative exponential correlation with permeability, with an initial slow increase followed by a rapid increase.

Figure 5a shows the curves of the permeability variation with confining pressure for fractured coal samples under different axial pressure conditions. When the axial pressure is

10 MPa and the confining pressure increases from 3 MPa to 10 MPa, the permeability of the coal rock decreases from 0.166 mD to 0.078 mD, representing a 53.01% reduction. When the axial pressure is 14 MPa and the confining pressure increases from 3 MPa to 10 MPa, the permeability of the coal rock decreases from 0.152 mD to 0.076 mD, corresponding to a 50% reduction. When the axial pressure is 18 MPa, and the confining pressure increases from 3 MPa to 10 MPa, the permeability of the coal rock decreases from 0.148 mD to 0.073 mD, representing a reduction of 50.68%.

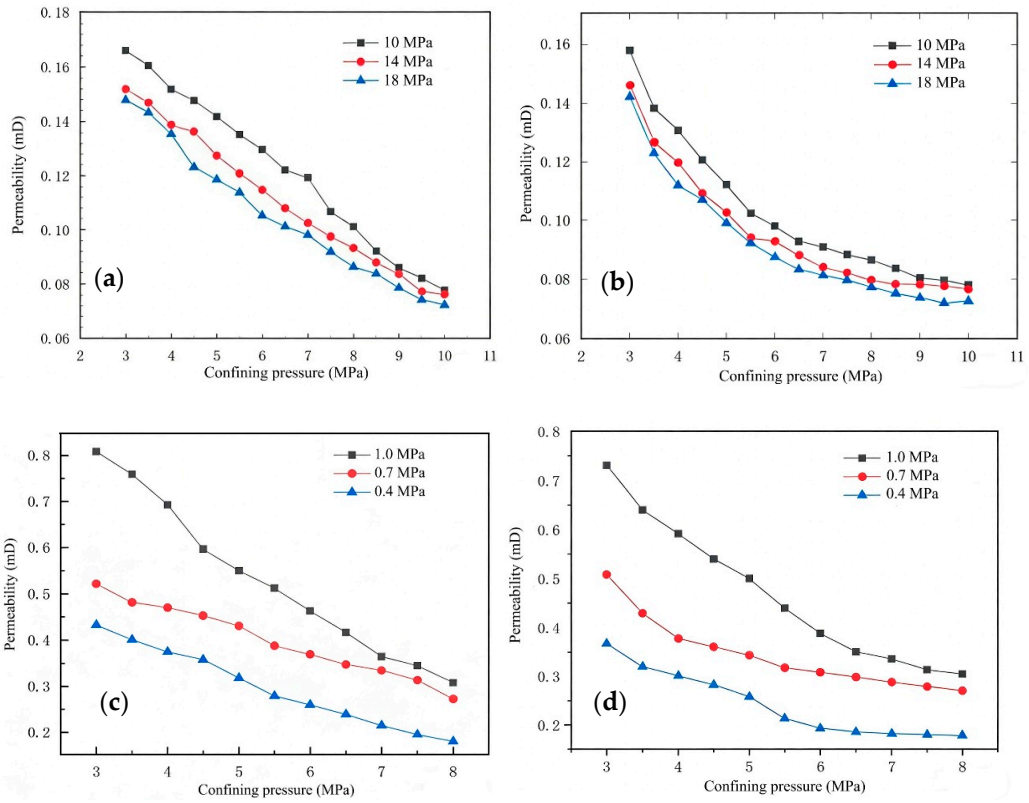

Figure 5. Permeability changes under different axial pressure and gas pressure conditions: (**a**) different axial pressure conditions during the loading process; (**b**) different axial pressure conditions during the unloading process; (**c**) different gas pressure conditions during the loading process; (**d**) different gas pressure conditions during the unloading process.

As shown in Figure 5b, when the axial pressure is 10 MPa and the confining pressure decreases from 10 MPa to 3 MPa, the permeability of the coal rock increases from 0.078 mD to 0.156 mD, representing an increase of 100%. When the axial pressure is 14 MPa and the confining pressure decreases from 10 MPa to 3 MPa, the permeability of the coal rock increases from 0.076 mD to 0.146 mD, corresponding to a 92.11% increase. When the axial pressure is 18 MPa and the confining pressure decreases from 10 MPa to 3 MPa, the permeability of the coal rock increases from 0.073 mD to 0.142 mD, representing a 94.52% increase. Therefore, regardless of the magnitude of the axial pressure, as the confining pressure increases, the permeability of the coal rock decreases linearly. Conversely, as the confining pressure decreases, the permeability of the coal rock continuously increases, exhibiting exponential growth.

When the confining pressure is 10 MPa, the permeability increases by 4.11% as the axial pressure decreases from 18 MPa to 14 MPa, and it increases 2.63% as the axial pressure decreases from 14 MPa to 10 MPa. When the confining pressure is 3 MPa, the permeability increases it increases 2.82% as the axial pressure decreases from 18 MPa to 14 MPa, and by 6.85% as the axial pressure decreases from 14 MPa to 10 MPa. This indicates that, under

the same confining pressure conditions, permeability improves slightly with every 4 MPa reduction in the axial pressure, with the increase ranging from approximately 0 to 10%. Therefore, it can be concluded that changes in confining pressure have a greater impact on coal rock permeability than changes in axial pressure.

As shown in Figure 5c,d, when the confining pressure is 8 MPa, and the gas pressure increases from 0.4 MPa to 0.7 MPa, the permeability of the coal rock increases from 0.178 mD to 0.271 mD, representing a permeability change rate of 52.25%. When the gas pressure increases from 0.7 MPa to 1 MPa, permeability increases from 0.271 mD to 0.305 mD, corresponding to a 12.55% increase. When the confining pressure is 3 MPa, and the gas pressure increases from 0.4 MPa to 0.7 MPa, the permeability increases from 0.367 mD to 0.508 mD, with a permeability change rate of 38.42%. When the gas pressure increases from 0.7 MPa to 1 MPa, the permeability rises from 0.508 mD to 0.730 mD, yielding a 30.41% increase. In summary, as the gas pressure increases, permeability also increases. For every 0.3 MPa increase in gas pressure, permeability increases by approximately 10% to 50%.

3.2. Permeability Recovery and Stress Sensitivity of Coal Rock During Unloading Process

To further analyze the impact of stress changes on permeability, the relationship between the permeability change and stress was examined by introducing the permeability recovery rate, permeability damage rate, and stress sensitivity coefficient, as shown in Equations (4), (5) and (6), respectively.

The permeability recovery rate is:

$$D_r = \frac{k_i - k_0}{k_0} \times 100\% \tag{4}$$

The permeability damage rate is:

$$D_k = \frac{k_0 - k_i}{k_0} \times 100\% \tag{5}$$

The stress sensitivity coefficient [36] is:

$$C_k = -\frac{1}{k_o}\frac{\Delta_k}{\Delta_{\sigma_e}} \tag{6}$$

where D_r represents the permeability recovery rate during the confining pressure reduction stage; D_k represents the permeability damage rate during the confining pressure increase stage; k_i denotes the permeability corresponding to the i-th confining pressure loading (or unloading), measured in mD; k_0 is the permeability of the coal sample corresponding to the initial stress loading state, measured in mD; and Δ_{σ_e} represents the change value of stress, measured in MPa.

As shown in Figure 6a, regardless of the changes in axial pressure, the permeability damage rate exhibits the following trend: as the confining pressure increases, the damage rate increases linearly. Moreover, the lower the axial pressure, the higher the rate of permeability damage. Specifically, for every 4 MPa reduction in the axial pressure, the permeability damage rate increases by approximately 1%.

As shown in Figure 6b, the lower the axial pressure, the higher the permeability recovery rate. For every 4 MPa reduction in the axial pressure, the permeability recovery rate increases by approximately 6%. Regardless of the changes in the axial pressure, the permeability recovery rate shows a gradually increasing trend as the confining pressure decreases. At lower confining pressures, the permeability recovery rate changes more rapidly, while at higher confining pressures, it changes more slowly.

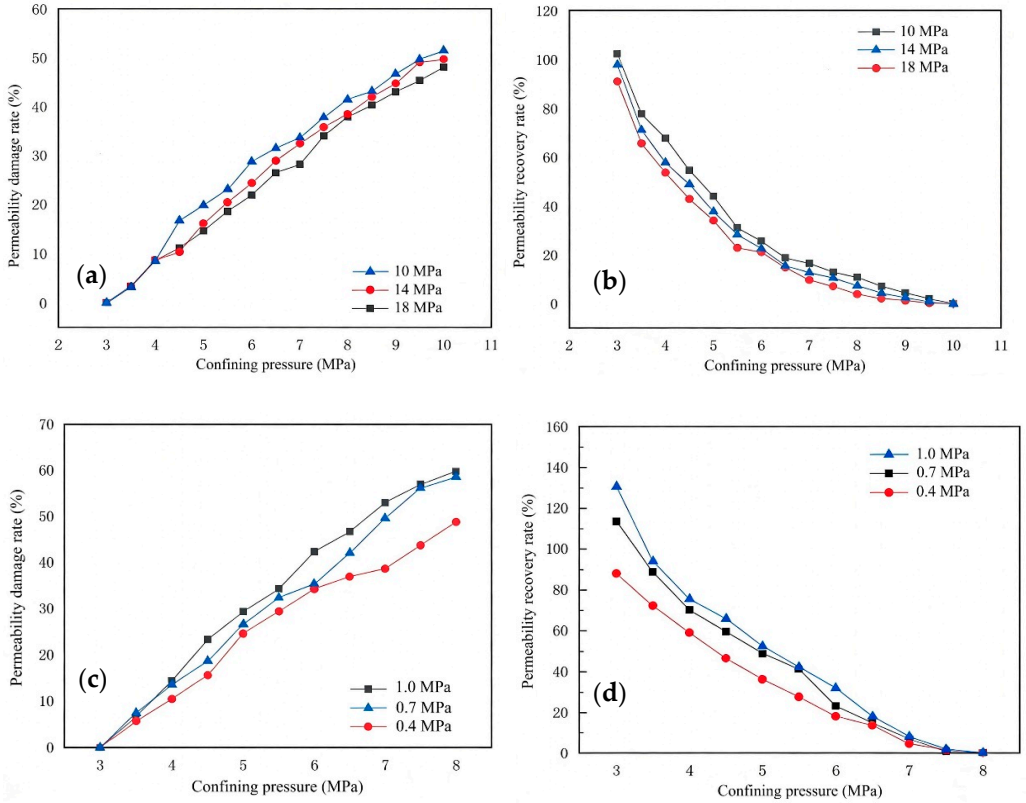

Figure 6. Permeability recovery and damage rates under different axial pressure and gas pressure conditions: (**a**) permeability recovery rate under different axial pressure conditions; (**b**) permeability damage rate under different axial pressure conditions; (**c**) permeability damage rate under different gas pressure conditions; (**d**) permeability recovery rate under different gas pressure conditions.

As shown in Figure 6c, the higher the gas pressure, the greater the permeability damage rate during loading. Specifically, for every 0.3 MPa increase in the gas pressure, the permeability damage rate increases by approximately 0–10%. As shown in Figure 5d, the higher the gas pressure, the greater the permeability recovery rate during unloading. For every 0.3 MPa increase in the gas pressure, the permeability recovery rate increases by approximately 20%.

In Figure 7b, it can be observed that as the gas pressure increases, the stress sensitivity coefficient also increases, indicating enhanced stress sensitivity of the coal rock. For every 0.3 MPa increase in the gas pressure, the stress sensitivity coefficient increases by approximately 0.04.

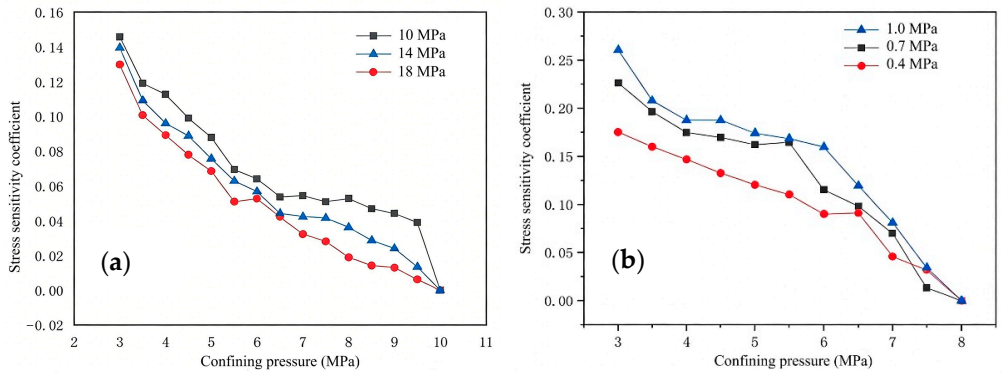

Figure 7. Variations in the stress sensitivity coefficient under different axial pressure and gas pressure conditions: (**a**) different axial pressure conditions; (**b**) different gas pressure conditions.

These findings suggest that during hydraulic slotting for CBM depressurization development, the magnitude of the reservoir pressure also influences the variation in coal seam permeability during depressurization. Moreover, higher reservoir pressure is more conducive to improving coal seam permeability during depressurization.

3.3. Implications of Permeability Variation for Permeability Enhancement Through Hydraulic Slotting in Deep Coal Seams

During deep CBM development, high-pressure water-jet slotting is performed along horizontal boreholes (typically oriented along the maximum horizontal principal stress direction), creating slots or cavities perpendicular to the boreholes within the coal seam [37]. The formation of these slots or cavities can induce significant in situ stress release, thereby generating numerous tensile fractures around the slots. In this scenario, permeability exhibits exponential growth, facilitating CBM migration (Figure 8).

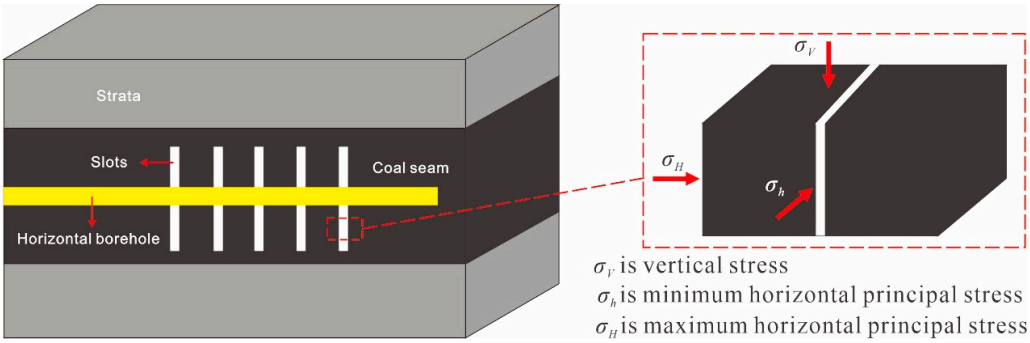

Figure 8. Mechanism of permeability enhancement through hydraulic slotting for in situ stress release in deep CBM wells.

The permeability test results indicate that the permeability of the fractured coal sample is more than 10 times that of the intact coal sample. The results of the loading and unloading experiments on confining and axial pressures show that the stress release in the coal seam can significantly enhance the permeability of CBM reservoirs. This suggests that hydraulic slotting may significantly enhance the permeability of deep coal seams. In addition, based on the permeability enhancement laws of fractured coal rock under different injected gas pressure conditions, higher gas pressure results in greater permeability and higher permeability recovery rates. This is because higher gas pressure can provide a more effective support for diversion fractures, which is beneficial for improving the permeability of the reservoir. Well test data from deep CBM reservoirs indicate that reservoir pressures can reach over 20 MPa, significantly higher than those in shallow CBM reservoirs (typically 3–8 MPa). This suggests that the permeability enhancement effects of slotting and pressure relief in deep CBM reservoirs may be superior to those in shallow coal seams. Due to limitations in the experimental conditions, the gas pressure used in the laboratory is far lower than that in the actual formation. For deep formations with pressures exceeding 10 MPa, the recovery pattern of reservoir permeability remains incompletely understood, and further research is required.

4. Conclusions

Coal samples obtained from the Linxing–Shenfu mining area in the Eastern Margin of the Ordos Basin, China, were used to conduct CBM seepage experiments under varying stress states. The permeability variations in coal rock under different confining, axial, and gas pressures were measured. The main conclusions are as follows:

(1) During the loading process, coal rock compression leads to the closure of pores and fractures, resulting in a decrease in permeability with increasing confining pressure. During unloading, coal rock undergoes expansion and deformation, and its permeability increases with decreasing confining pressure. The change in permeability transitions from slow to rapid, and the stress sensitivity coefficient of coal rock increases, indicating enhanced stress sensitivity.

(2) The permeability enhancement law of fractured coal rock under different axial pressure conditions reveals that, regardless of the loading or unloading process, lower axial pressure results in higher permeability, greater permeability recovery and damage rates, a larger stress sensitivity coefficient, and stronger stress sensitivity of the coal rock.

(3) The permeability enhancement law of fractured coal rock under different injected gas pressure conditions indicates that higher gas pressure leads to greater permeability, higher permeability recovery and damage rates, a larger stress sensitivity coefficient, and stronger stress sensitivity of the coal rock.

In practical deep CBM reservoir stimulation, the crushing and slotting process involves complex stress change behavior resulting from simultaneous changes in multiple directions. Therefore, future research will involve collecting cubic rock specimens and conducting true triaxial experiments to study the laws governing permeability variation in fractured coal rock under different stress change paths. In addition, a higher pressure and higher temperature will be considered in the experiments to bring the experimental conditions closer to the environment of deep CBM reservoirs.

Author Contributions: Conceptualization, R.L.; methodology, L.J. and R.L.; validation, J.H. and L.J.; formal analysis, J.H. and L.J.; investigation, B.Y. and L.Z.; resources, R.L.; data curation, L.J.; writing—original draft preparation, L.J. and J.H.; writing—review and editing, R.L.; visualization, L.Z.; supervision, R.L.; project administration, R.L.; funding acquisition, R.L. All authors have read and agreed to the published version of the manuscript.

Funding: This research was funded by the National Key Research and Development Program of China (grant number 2023YFC3009001), the National Natural Science Foundation of China (grant number U19B2009).

Data Availability Statement: All data generated or analyzed during this study are included in this published article.

Acknowledgments: The authors acknowledge the support provided by Chongqing University for providing basic facilities to accomplish this work.

Conflicts of Interest: The author Jingjing Huo was employed by the Lu'An Chemical Group Co., Ltd. The remaining authors declare that the research was conducted in the absence of any commercial or financial relationships that could be construed as potential conflicts of interest.

References

1. Karacan, C.Ö.; Goodman, G.V.R. Analyses of Geological and Hydrodynamic Controls on Methane Emissions Experienced in a Lower Kittanning Coal Mine. *Int. J. Coal Geol.* **2012**, *98*, 110–127. [CrossRef]
2. Zhu, Q.; Du, X.; Zhang, T.; Yu, H.; Liu, X. Investigation into the variation characteristics and influencing factors of coalbed methane gas content in deep coal seams. *Sci. Rep.* **2024**, *14*, 18813. [CrossRef] [PubMed]
3. Kędzior, S.; Teper, L. Coal Properties and Coalbed Methane Potential in the Southern Part of the Upper Silesian Coal Basin, Poland. *Energies* **2023**, *16*, 3219. [CrossRef]
4. Peng, G. Fracture Propagation Laws of Staged Hydraulic Fracture in Fractured Geothermal Reservoir Based on Phase Field Model. *Int. J. Coal Sci. Technol.* **2023**, *10*, 52. [CrossRef]
5. Li, S.; Qin, Y.; Tang, D.; Shen, J.; Wang, J.; Chen, S. A comprehensive review of deep coalbed methane and recent developments in China. *Int. J. Coal Geol.* **2023**, *279*, 104369. [CrossRef]

6. Li, R.; Zhang, L.; Xie, J.; Chen, Z.; Yang, B.; Xiang, W.; Zhai, X. A Study on the Controlling Effect of Geological Structures on Coalbed Methane Occurrence in the Northeast Margin of Qinshui Basin, North China. *Energies* **2025**, *18*, 647. [CrossRef]
7. Adib, A.; Afzal, P.; Ilani, S.M.; Aliyari, F. Determination of the Relationship between Major Fault and Zinc Mineralization Using Fractal Modeling in the Behabad Fault Zone, Central Iran. *J. Afr. Earth Sci.* **2017**, *134*, 308–319. [CrossRef]
8. Salmachi, A.; Rajabi, M.; Wainman, C.; Mackie, S.; McCabe, P.; Camac, B.; Clarkson, C. History, Geology, In Situ Stress Pattern, Gas Content and Permeability of Coal Seam Gas Basins in Australia: A Review. *Energies* **2021**, *14*, 2651. [CrossRef]
9. Uliasz-Misiak, B.; Misiak, J.; Lewandowska-Śmierzchalska, J.; Matuła, R. Environmental Risk Related to the Exploration and Exploitation of Coalbed Methane. *Energies* **2020**, *13*, 6537. [CrossRef]
10. Guo, X.; Li, Y.; Pan, Y.; Wang, A.; Huang, B. Numerical Simulation of the Rock-Breaking Mechanism for Heterogeneous Rock with High-Voltage Electrical Pulse. *Rock Mech. Rock Eng.* **2025**, *58*, 9193–9211. [CrossRef]
11. Gray, I. Reservoir engineering in coal seams: Part 1—The physical process of gas storage and movement in coal seams. *SPE Reserv. Eng.* **1987**, *2*, 28–34. [CrossRef]
12. Palmer, I.; Mansoori, J. How permeability depends on stress and pore pressure in coalbeds: A new model. *SPE Reserv. Eval. Eng.* **1998**, *1*, 539–544. [CrossRef]
13. Shi, J.Q.; Durucan, S. Drawdown induced changes in permeability of coalbeds: A new interpretation of the reservoir response to primary recovery. *Transp. Porous Media* **2004**, *56*, 1–16. [CrossRef]
14. Harpalani, S.; Chen, G. Influence of gas production induced volumetric strain on permeability of coal. *Geotech. Geol. Eng.* **1997**, *15*, 303–325. [CrossRef]
15. Robertson, E.P.; Christiansen, R.L. A permeability model for coal and other fractured, sorptive-elastic media. *SPE J.* **2007**, *12*, 314–324. [CrossRef]
16. Chen, D.; Pan, Z.; Liu, J.; Connell, L.D. An improved relative permeability model for coal reservoirs. *Int. J. Coal Geol.* **2013**, *109*, 45–57. [CrossRef]
17. Wang, S.; Elsworth, D.; Liu, J. Permeability evolution during progressive deformation of intact coal and implications for instability in underground coal seams. *Int. J. Rock Mech. Min. Sci.* **2014**, *68*, 34–45. [CrossRef]
18. Porfido, C.; Rizzo, R.E.; Healy, D.; Spagnuolo, M.; Terzano, R.; Allegretta, I. Investigating the evolution of fractures in clay-based ceramics during repeated freeze-thawing cycles using X-ray micro-computed tomography and image analysis. *Mater. Charact.* **2021**, *177*, 111185. [CrossRef]
19. Chen, Y.; Hu, S.; Wei, K.; Hu, R.; Zhou, C.; Jing, L. Experimental characterization and micromechanical modeling of damage-induced permeability variation in Beishan granite. *Int. J. Rock Mech. Min. Sci.* **2014**, *71*, 64–76. [CrossRef]
20. Zhao, Z.; Liu, P.; Li, Q.; Nie, B.; Song, J.; Bao, J.; He, H.; Liu, W.; Sun, L. Enhancing coalbed methane recovery using high power ultrasonic excitation: A nano-micro -to-engineering scale study. *Energy* **2025**, *320*, 135274. [CrossRef]
21. Cao, W.; Lei, Q.; Cai, W. Stress-Dependent Deformation and Permeability of a Fractured Coal Subject to Excavation-Related Loading Paths. *Rock Mech. Riock. Eng.* **2021**, *54*, 4299–4320. [CrossRef]
22. Wang, D.; Zeng, F.; Wei, J.; Zhang, H.; Wu, Y.; Wei, Q. Quantitative analysis of fracture dynamic evolution in coal subjected to uniaxial and triaxial compression loads based on industrial CT and fractal theory. *J. Petro. Sci. Eng.* **2021**, *196*, 108051. [CrossRef]
23. Li, J.; Li, B.; Wang, Z.; Ren, C.; Yang, K.; Gao, Z. A permeability model for anisotropic coal masses under different stress conditions. *J. Petro. Sci. Eng.* **2021**, *198*, 108197. [CrossRef]
24. Zhou, H.; Zhang, L.; Wang, X.; Rong, T.; Wang, L. Effects of matrix-fracture interaction and creep deformation on permeability evolution of deep coal. *Int. J. Rock Mech. Min. Sci.* **2020**, *127*, 104236. [CrossRef]
25. Sudakov, O.; Burnaev, E.; Koroteev, D. Driving digital rock towards machine learning: Predicting permeability with gradient boosting and deep neural networks. *Comput. Geosci.* **2019**, *127*, 91–98. [CrossRef]
26. Zhang, H.; Zhang, J.; Du, S.; Ren, J.; Zhao, H.; Li, W.; Ding, M.; Wang, T. Permeability Characteristics of Filled Fractured Coal-Rock Mass Under Stress–Seepage Coupling. *Rock Mech. Rock Eng.* **2025**, *58*, 11899–11920. [CrossRef]
27. Yang, F.; Li, B.; Wang, K.; Wen, H.; Yang, R.; Huang, Z. Extreme massive hydraulic fracturing in deep coalbed methane horizontal wells: A case study of the Linxing Block, eastern Ordos Basin, NW China. *Pet. Explor. Dev.* **2024**, *51*, 440–452. [CrossRef]
28. Zhang, K.; Li, S.; Zhong, G.; Feng, P.; Chang, C.; Li, H. Characteristics of in-situ stress field of coalbed methane reservoir in the eastern margin of Ordos basin. *Int. J. Coal Geol.* **2025**, *301*, 104715. [CrossRef]
29. Li, R.; Lu, Y.; Xia, B.; Chen, W.; Sun, H. Characteristics of in situ stress and reservoir pressure in deep coal seams and their influences on reservoir depletion: A field case study. *Geofluids* **2023**, *2023*, 1622612. [CrossRef]
30. Chen, Y.; Tang, D.; Xu, H.; Li, Y.; Meng, Y. Structural controls on coalbed methane accumulation and high production models in the eastern margin of Ordos Basin, China. *J. Nat. Gas Sci. Eng.* **2015**, *23*, 524–537. [CrossRef]
31. Liu, C.; Liu, Q.; Lv, B.; Han, P.; Wang, L.; Cheng, Y. Impact of Stress on Adsorption–Desorption Hysteresis in Coal: Effect of Desorption Driving Force on Flowable CH_4. *Energy Fuels* **2025**, *39*, 18476–18490. [CrossRef]
32. Ge, Z.; Zhong, J.; Lu, Y.; Cheng, L.; Zheng, J.; Zhou, Z.; Cheng, Y. Directional distance prediction model of slotting–directional hydraulic fracturing (SDHF) for coalbed methane (CBM) extraction. *J. Pet. Sci. Eng.* **2019**, *183*, 106429. [CrossRef]

33. Wang, K.; Zhang, G.; Du, F.; Wang, Y.; Yi, L.; Zhang, J. Simulation of directional propagation of hydraulic fractures induced by slotting based on discrete element method. *Petroleum* **2023**, *9*, 592–606. [CrossRef]
34. Mi, L.; Zhu, G. Geological characteristics and exploration breakthrough in Linxing-Shenfu tight gas field, northeastern Ordos Basin. *China Pet. Explor.* **2021**, *26*, 53–67. (In Chinese) [CrossRef]
35. Liu, J.; Zhu, G.; Liu, Y.; Chao, W.; Du, J.; Yang, Q.; Mi, H.; Zhang, S. Breakthrough, future challenges and countermeasures of deep coalbed methane in the eastern margin of Ordos Basin: A case study of Linxing-Shenfu block. *Acta Pet. Sin.* **2023**, *44*, 1827–1839. (In Chinese) [CrossRef]
36. Xiao, K.; Zhang, Z.; Zhang, R.; Gao, M.; Xie, J.; Zhang, A.; Liu, Y. Anisotropy of the effective porosity and stress sensitivity of coal permeability considering natural fractures. *Energy Rep.* **2021**, *7*, 3898–3910. [CrossRef]
37. Li, R.; Li, G. Coalbed methane industry development framework and its limiting factors in China. *Geofluids* **2022**, *2022*, 8336315. [CrossRef]

Disclaimer/Publisher's Note: The statements, opinions and data contained in all publications are solely those of the individual author(s) and contributor(s) and not of MDPI and/or the editor(s). MDPI and/or the editor(s) disclaim responsibility for any injury to people or property resulting from any ideas, methods, instructions or products referred to in the content.